
E^2 PN: Efficient SE(3)-Equivariant Point Network

Minghan Zhu

University of Michigan
Ann Arbor, MI 48109
minghanz@umich.edu

Maani Ghafarri

University of Michigan
Ann Arbor, MI 48109
maanigj@umich.edu

William A Clark

Cornell University
Ithaca, NY 14850
wac76@cornell.edu

Huei Peng

University of Michigan
Ann Arbor, MI 48109
hpeng@umich.edu

Abstract

This paper proposes a new point-cloud convolution structure that learns SE(3)-equivariant features. Compared with existing SE(3)-equivariant networks, our design is lightweight, simple, and flexible to be incorporated into general point-cloud learning networks. We strike a balance between the complexity and capacity of our model by selecting an unconventional domain for the feature maps. We further reduce the computational load by properly discretizing \mathbb{R}^3 to fully leverage the rotational symmetry. Moreover, we employ a permutation layer to recover the full SE(3) group from its quotient space. Experiments show that our method achieves comparable or superior performance in various tasks while consuming much less memory and running faster than existing work. The proposed method can foster the adoption of equivariant feature learning in various practical applications based on point clouds and inspire future developments of equivariant feature learning for real-world applications.

1 Introduction

Processing 3D data has become a vital task today as demands for automated robots and augmented reality technologies continuously emerge. While computer vision has hugely succeeded in processing image data, learning on 3D data is more challenging. One important reason is that 3D data presents more variations than 2D images in several aspects. For example, the rigid body transformations in 2D space only have 2 degrees of freedom for translations and 1 degree of freedom for rotations. In 3D space, the degrees of freedom are 3 for translations and 3 for rotations. The sliding-window mechanism enabling the 2D translation equivariance is a key factor in the success of convolutions in 2D image processing because it enables parameter sharing and generalization across 2D translations.

Loosely speaking, *equivariance* is a property for a map such that given a transformation in the input, the output changes in a predictable way determined by the input transformation. It drastically improves generalization as the variance caused by the transformations is captured via the network by design. In the example above, the equivariance property boils down to the fact that a translation in the input image results in the same translation in the feature map output from a conv layer. However, a conventional convolution layer is not equivariant to rotations, which becomes problematic, primarily when we deal with 3D data, where many rotational variations occur. In response, on the one hand, data augmentations with 3D rotations are frequently used. On the other hand, equivariant feature learning emerges as a research area, aiming to generalize the translational equivariance to broader transformations. We will mainly discuss equivariant feature learning, to which our work also belongs.

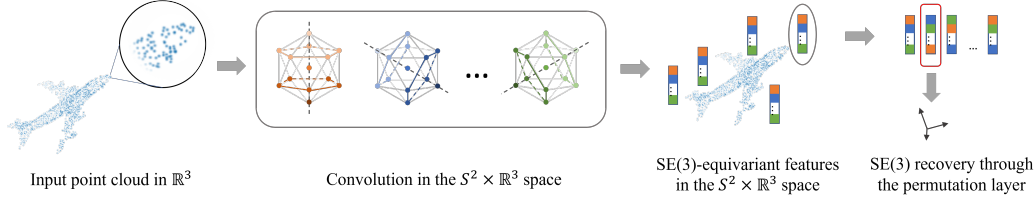


Figure 1: A high-level illustration of our network. We lift the convolution to $S^2 \times \mathbb{R}^3$, which is a rare choice for SE(3)-equivariant feature learning. The different colors represent channels in S^2 . Details in Sec. 4.

A lot of progress has been made in group-equivariant feature learning. The term *group* encompasses the 3D rotations and translations, which is called the special Euclidean group of dimension 3, denoted SE(3), and also other more general types of transformations that represent certain symmetries. While many methods have been proposed to learn features equivariant to various transformations, equivariant feature learning has not become the default go-to strategy in 3D data learning tasks yet. From our understanding, two major reasons hinder the broader application of equivariant methods. First, networks dealing with continuous groups typically requires specially designed operations that are not commonly used in neural networks. For example, Harmonic functions and generalized Fourier Transforms are frequently used in SO(2)- and SO(3)-equivariant learning [1–3]. Thus it is challenging to incorporate them into general neural networks for 3D learning tasks. Second, for the strategy of working on a discretization of the continuous groups [4, 5], while the network structures are generally simpler and closer to conventional networks, they usually suffer from the high dimensionality of feature maps and convolutions, which causes much larger memory consumption and computational load, limiting their practical use.

In this work, we tackle this problem and design a convolution structure for processing 3D point clouds, one of the most common forms of 3D data today. Our proposed structure, shown in Fig. 1, works on a discretization of SE(3) so that it is more compatible with conventional neural networks. Meanwhile, we resolve the problem of high dimensionality by defining feature maps not on the (discretized) SE(3) space but on a quotient space of SE(3), the $S^2 \times \mathbb{R}^3$ space (\times for Cartesian product). Furthermore, we improve the efficiency of convolutions by designing the kernels to be symmetric to the discretized rotations. We also propose a permutation layer to recover SE(3) information from the quotient space when poses are wanted. As a result, our proposed network is both SE(3)-equivariant (approximately up to the discretization) and efficient, ready for application in practical point-cloud learning tasks. Overall, this work has the following contributions:

- We propose an efficient SE(3)-equivariant convolution structure for 3D point clouds.
- We design a permutation layer to recover the full SE(3) information from its quotient space.
- We achieve comparable or better performance with largely reduced memory consumption and computational load compared with existing work.
- Our code will be open-sourced at <https://github.com/minghanz/E2PN>.

2 Preliminaries and notation

Groups A group G is a set equipped with a binary operator \cdot , satisfying the following conditions: (1) the set is closed under the operation: $x \cdot y \in G, \forall x, y \in G$; (2) the operation is associative: $x \cdot (y \cdot z) = (x \cdot y) \cdot z, \forall x, y, z \in G$; (3) there is an identity element e in the set such that $x \cdot e = e \cdot x = x, \forall x \in G$; (4) there is an inverse x^{-1} for each element x in the set such that $x \cdot x^{-1} = x^{-1} \cdot x = e$. For example, the interger set \mathbb{Z} is a group under the addition operator with identity 0 and inverse $-x$ for any $x \in \mathbb{Z}$. Sometimes we omit the \cdot notation.

Group actions and representations We say a group *acts* on a set X if any element g in G corresponds to a transformation $\rho(g)$ on X , i.e., $[\rho(g)](x) \in X, \forall x \in X$, such that $\rho(g_1) \circ \rho(g_2) = \rho(g_1 g_2), \forall g_1, g_2 \in G$, where \circ denotes function compositions, and $[\rho(e)](x) = x, \forall x \in X$. When X is a linear space and $\rho(g)$ is linear, we say ρ is a (linear) *representation* of G in X . When X is n (finite)-dimensional linear space, we have a representation $\rho : G \rightarrow \text{GL}(n)$, i.e., $[\rho(g)](x) = \rho_n(g)x$,

where $\rho_n(g)$ takes the form of n -by- n invertible matrices. For example, the representations of 2D rotations $\text{SO}(2)$ in \mathbb{R}^2 are the 2-by-2 orthonormal matrices with determinant 1. We denote $[\rho(g)](x)$ as $\rho(g)x$ as the actions used in this paper are applied on the left. We also use (ρ, X) as a shorthand to denote the representation and the space it acts on.

Equivariance Given spaces V_1 with representation ρ_1 of G and V_2 with representation ρ_2 of G , we say a mapping $\phi : V_1 \rightarrow V_2$ is G -equivariant if $\phi \circ \rho_1(g) = \rho_2(g) \circ \phi, \forall g \in G$. A G -equivariant linear map is also called an *intertwiner*. The space of intertwiners is denoted $\text{Hom}_G(\rho_1, \rho_2)$, homomorphisms of group representations ρ_1, ρ_2 of G .

Subgroups, cosets, and quotient spaces A subgroup H of G is a subset of G that is also a group, denoted $H \leq G$. For example, $\text{SO}(2) \leq \text{SO}(3)$. Given $H \leq G$ and $g \in G$, we can define a (left-)coset as $gH = \{gh|h \in H\}$. For a given H , all cosets are either equal or disjoint. Each coset is of the same size (contains the same number of elements), and they partition the whole group. The set of cosets form a coset space (or *quotient space*) $G/H = \{gH|g \in G\}$. A quotient space is generally not a group. In short, a coset is both a subset in the group and an element in the quotient space.

Homogeneous spaces Assume that a group G acts on a space X through action ρ , we call X a *homogeneous space* of G if G acts *transitively* on X , i. e., any two elements in X are connected by a group action, $\forall x_1, x_2 \in X, \exists g \in G, \text{ s.t. } x_1 = \rho(g)x_2$. Any quotient space is a homogeneous space of G , and for any homogeneous space X , $\exists H \leq G$ such that $X \cong G/H$, where H is also called the *stabilizer*, because H stabilizes the identity of X : $\rho(h)e_X = e_X, \forall h \in H$.

Induced representations Here is an important known result [6–8]: given a representation ρ of subgroup H on vector space V , one can *induce* a representation $\pi = \text{Ind}_H^G \rho$ of G for the space of functions $\mathcal{F} = \{f : G/H \rightarrow V\}$. It provides us a way to define group actions in function spaces, which is a foundation of the research on equivariant feature learning.

3 Review of existing work

Early efforts of equivariant feature learning focused on a special case of induced representation where the subgroup H only contains the identity element. In this case, the condition on the representation (ρ, V) of H becomes trivial, and we have a representation on the function space $\mathcal{F} = \{f : G \rightarrow V\}$ for free, which is called the *regular* representation. Normally, the input data live in a lower-dimensional space than (typically a homogeneous space of) the group G where we desire the equivariant property. For example, one may desire $\text{SO}(3)$ -rotational equivariance on spherical data. The sphere space $S^2 \cong \text{SO}(3)/\text{SO}(2)$ (\cong for isomorphism) is a homogeneous space of $\text{SO}(3)$. Therefore, one is required to *lift* the input domain X to G to have a proper representation on the feature function space. Lifting is usually accompanied with discretization of the group, since feature maps are typically realized as n -dim matrices with discrete indices. Once the feature maps are defined on G , naive convolutions over the domain G give G -equivariant mappings between network layers, as shown in [4]. Attention also works similarly [9]. Many works applied this strategy to learn group-equivariant features. For example, [4, 5] for $\text{SE}(2)$, [10] for $\text{SO}(3)$, [11, 12] for $\text{SE}(3)$, and [13] for $\text{E}(3)$ equivariance up to some discretization. Continuous convolution in the lifted domain is also possible through Fourier transforms [1] and B-splines [14], which we do not elaborate here.

A major problem of this strategy is that the lifting makes the network too large. The cardinality of the domain of feature maps grows exponentially with the number of dimensions. The size of feature maps and the computation complexity of convolutions grow linearly and quadratically with the domain cardinality, respectively, if the kernel is global. The problem gets more prominent when it comes to $\text{SE}(3)$ -equivariant learning. For example, EPN [12] lifts \mathbb{R}^3 to $\mathcal{I} \times \mathbb{R}^3$ where \mathcal{I} is a discretization of $\text{SO}(3)$ with 60 elements, rendering 60 times larger feature maps.

Another line of work is to stick to the input domain X and leverage the induced representation instead. The space of feature maps is $\mathcal{F} = \{f : X \rightarrow V\}$, which is the same as conventional non-equivariant networks, thus avoiding the problem caused by extended dimensions. The gap between X and the group of interest G is the stabilizer subgroup H s.t. $X = G/H$, and the representation (ρ, V) of H is a foundation for the representation $(\text{Ind}_H^G \rho, \mathcal{F})$. The representation of compact groups (which the stabilizers are) can be decomposed into a direct sum of *irreducible representations (irreps)*, according

to representation theory [15]. One may freely choose from the irreps to compose the representation ρ . However, the chosen ρ poses a restriction on the intertwiners. In other words, the convolution kernel is restricted to a specific form determined by ρ in order to make the convolution a G -equivariant mapping [8]. It could be cumbersome for subgroups H with complicated irreps. For example, TFN [3] learns SE(3)-equivariant feature maps on \mathbb{R}^3 induced from the stabilizer SO(3). The irreps of SO(3) are $(2l + 1) \times (2l + 1)$ Wigner-D matrices with non-negative integers l . One may stack vector spaces with different level l , and they interact through tensor product using Clebsch-Gordan coefficients $C^{lk} \in \mathbb{R}^{(2l+1)(2k+1) \times (2l+1)(2k+1)}$ for between level k and l . We also need spherical harmonics as basis of SO(3)-equivariant functions to express the kernels. More details can be found in [3, 16]. It has become a standard way for SE(3)-equivariant feature learning, with following work building modifications and generalizations upon it [17–19]. However, the computation is rather involved and gets expensive for large l . As the learnable part of the kernel is only some radial functions with a scalar input, such convolutions have limited flexibility while being complicated.

In the literature, the above work is typically classified into G -CNNs and *Steerable G-CNNs* [8, 14], depending on whether a method lifts the domain of its feature maps to the full group G or extend the codomain of feature maps to be steerable by ρ . However, we view the difference as different selections of the stabilizer H . G-CNNs work with $H = \{I\}$, while steerable G-CNNs work with H such that the input domain $X = G/H$. This viewpoint sheds light on new opportunities. As introduced below, we pick a new H , which is the key differentiator of our method and leads to a new form of feature maps and convolutions. This new form is lightweight and easy to use without sacrificing the performance.

4 Our method

4.1 Background

Our convolution structure is built upon KPConv [20]. Here is a brief recap. KPConv defines the convolution kernel on a set of kernel points in the 3D space: $\kappa : \overline{\mathbb{R}^3} \rightarrow \mathbb{R}^{c_{out} \times c_{in}}$, where $\overline{\mathbb{R}^3} = \{t_1, \dots, t_n \in \mathbb{R}^3\}$ is the set of kernel points. We use $\bar{\cdot}$ (a top bar) to denote the discretization of a group or space. When calculating the feature at a certain point, the kernel is centered at that location, and all kernel points gather features from their neighboring input points through weighted sum. The convolution is then conducted on the gathered features. Denoting convolutions (precisely cross-correlations) as $*$, we have:

$$[\kappa * f](x) = \int_{\overline{\mathbb{R}^3}} \kappa(t) f'(x+t) dt = \sum_{i=1}^n \kappa(t[i]) f'(x+t[i]), \quad (1)$$

where $f'(x) = \sum_{x_j \in \mathcal{N}_x} f(x_j) w(x_j - x)$ is the feature gathered at x from the set of neighboring points \mathcal{N}_x using a distance-based weighting function w . Notice that the kernel is defined at a fixed set of discretized locations, while the input and output feature maps can be queried arbitrarily in \mathbb{R}^3 .

To extend the convolution to a general homogeneous space, we need one more concept. A binary operation is not defined between two elements in a homogeneous space because a homogeneous space is generally not a group. Thus we introduce a *section* function $s : G/H \rightarrow G$, s.t.

$$s(x)H = x, \forall x \in G/H, \quad (2)$$

meaning that s maps a coset to an element of G in that coset. In this way, an element in the homogeneous space may "acts" on the other given an s function. Now we can generally formulate the convolution in a homogeneous space:

$$[\kappa * f](x) = \int_{G/H} \kappa(y) f(s(x)y) dy, \quad x \in G/H, \quad (3)$$

where dy is a Haar measure of G/H .

4.2 Overview of the convolution

On the high level, we choose SO(2) as the stabilizer and work with feature maps defined on the domain $\tilde{X} = \text{SE}(3)/\text{SO}(2)$ which is homeomorphic to the Cartesian product $S^2 \times \mathbb{R}^3$. Now we

extend the KPConv [20] from \mathbb{R}^3 to the domain $S^2 \times \mathbb{R}^3$. We discretize $\text{SO}(3)$ into the icosahedral rotation group \mathcal{I} with 60 elements (following EPN [12]), containing all rotational symmetries of an icosahedron. $\text{SO}(2)$ is discretized as the group of multiples of 72° planar rotations, which is a cyclic group of degree 5. Then we obtain a discretization of the sphere $\overline{S^2} = \text{SO}(3)/\text{SO}(2)$ of size 12 corresponding to the vertices of an icosahedron. The domain of a kernel is $\overline{S^2} \times \mathbb{R}^3$, while the domain of feature maps is $\overline{S^2} \times \mathbb{R}^3$, since a feature map can be queried at arbitrary spatial locations.

Denote an element in $\text{SO}(3)$ as R , an element in $\text{SO}(2)$ as R_z , an element in S^2 as $R\mathbf{n}$ where \mathbf{n} represents the north pole unit vector. Then we denote an element in the discretized sets $R[i]$, $R_z[i]$, and $R_{\mathbf{n}}[i]$ correspondingly. We further denote an element in $\text{SE}(3)$ as (R, t) , an element in $S^2 \times \mathbb{R}^3$ as $(R\mathbf{n}, t)$, and the group $\text{SE}(3)$ acts on $S^2 \times \mathbb{R}^3$ following: $(R_g, t_g)(R\mathbf{n}, t) = (R_g R\mathbf{n}, R_g t + t_g)$. We also need to define the section functions before formulating the convolution. The specific choice of $s : S^2 \rightarrow \text{SO}(3)$ and $\overline{s} : \overline{S^2} \rightarrow \mathcal{I}$ is elaborated in the appendix, but we denote $s(R\mathbf{n}) \triangleq R'$ and $\overline{s}(R_{\mathbf{n}}[i]) \triangleq R'[i]$ as shorthands. We slightly abuse the notation for section $s : S^2 \times \mathbb{R}^3 \rightarrow \text{SE}(3)$ as $s((R\mathbf{n}, t)) = (s(R\mathbf{n}), t)$, and $\overline{s} : \overline{S^2} \times \mathbb{R}^3 \rightarrow \overline{\text{SO}(3)} \times \mathbb{R}^3$ as $\overline{s}((R_{\mathbf{n}}[i], t)) = (\overline{s}(R_{\mathbf{n}}[i]), t)$.

In the continuous case, define the kernel $\kappa : S^2 \times \mathbb{R}^3 \rightarrow \mathbb{R}^{c_{out} \times c_{in}}$, and the convolution can be written as:

$$\begin{aligned} [\kappa * f]((R_p \mathbf{n}, t_p)) &= \int_{S^2 \times \mathbb{R}^3} \kappa((R_q \mathbf{n}, t_q)) f(s((R_p \mathbf{n}, t_p))(R_q \mathbf{n}, t_q)) d(R_q \mathbf{n}, t_q) \\ &= \int_{S^2 \times \mathbb{R}^3} \kappa((R_q \mathbf{n}, t_q)) f((R'_p, t_p)(R_q \mathbf{n}, t_q)) d(R_q \mathbf{n}, t_q) \\ &= \int_{S^2 \times \mathbb{R}^3} \kappa((R_q \mathbf{n}, t_q)) f((R'_p R_q \mathbf{n}, R'_p t_q + t_p)) d(R_q \mathbf{n}, t_q) \end{aligned} \quad (4)$$

In the discretized setup, we reuse the notation κ for $\kappa : \overline{S^2} \times \mathbb{R}^3 \rightarrow \mathbb{R}^{c_{out} \times c_{in}}$ since we will only use discretized kernels afterwards in the paper. The convolution can be written as:

$$\begin{aligned} [\kappa * f]((R_{\mathbf{n}}[i_p], t_p)) &= \sum_{i_q} \sum_{j_q} \kappa((R_{\mathbf{n}}[i_q], t[j_q])) f'(\overline{s}((R_{\mathbf{n}}[i_p], t_p))(R_{\mathbf{n}}[i_q], t[j_q])) \\ &= \sum_{i_q} \sum_{j_q} \kappa((R_{\mathbf{n}}[i_q], t[j_q])) f'((R'[i_p], t_p)(R_{\mathbf{n}}[i_q], t[j_q])) \\ &= \sum_{i_q} \sum_{j_q} \kappa((R_{\mathbf{n}}[i_q], t[j_q])) f'((R_{\mathbf{n}}[i'_q], R'[i_p] t[j_q] + t_p)) \end{aligned} \quad (5)$$

where i'_q is defined such that $R_{\mathbf{n}}[i'_q] = R[i'_p] R_{\mathbf{n}}[i_q] \in \overline{S^2}$. We know such i'_q exists because $\overline{S^2}$ is closed under actions of $\overline{\text{SO}(3)}$. $f'((R_{\mathbf{n}}[i], t)) = \sum_{t_j \in \mathcal{N}_i} f(R_{\mathbf{n}}[i], t_j) w(t_j - t)$ is the feature gathered from the neighboring input points \mathcal{N}_i .

So far we have not considered the constraints on the kernel κ posed by the representation ρ of the subgroup H ($\text{SO}(2)$ or $\overline{\text{SO}(2)}$) to make the convolution a valid intertwiner. In this paper, we simply use the trivial representation $\rho(h) = \text{Id}, \forall h \in H$, the identity transform. Denote $t = t(x, y, z)$ specifying its coordinates in \mathbb{R}^3 , the resulting constraint on the kernel can be written as:

$$\kappa(R\mathbf{n}, t(x_1, y_1, z_1)) = \kappa(R\mathbf{n}, t(x_2, y_2, z_2)) \quad \text{if } x_1^2 + y_1^2 = x_2^2 + y_2^2 \text{ and } z_1 = z_2 \quad (6)$$

Geometrically, this constraint can be understood as for any fixed $R\mathbf{n}$, $\kappa(R\mathbf{n}, \cdot)$ has a constant value on any circle centered around the z -axis in \mathbb{R}^3 . It also applies to the discretized case. The derivation of this constraint is presented in the appendix.

It turns out the restriction of (6) still leaves a lot of flexibility for the kernel, so that the convolution is able to extract rich features even if we use a trivial representation for the $\text{SO}(2)$ subgroup. Meanwhile, the dimensionality of the feature map is drastically reduced compared with G-CNNs (in this example, $|\overline{S^2}| = 12$ versus $|\mathcal{I}| = 60$). They are the results of picking the $\text{SO}(2)$ stabilizer subgroup and working with feature maps defined on the domain $S^2 \times \mathbb{R}^3$.

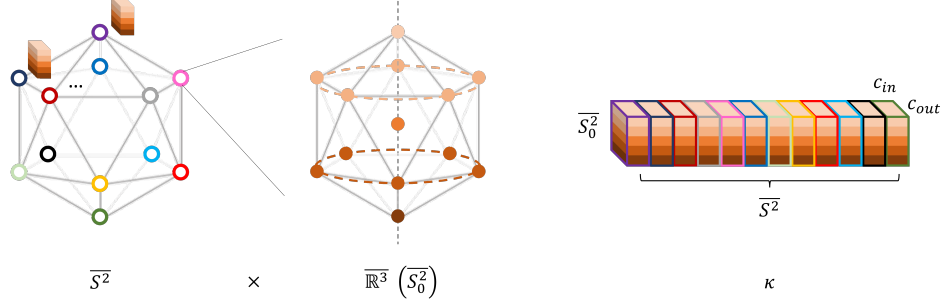


Figure 2: Illustration of the convolution kernel $\kappa : \overline{S^2} \times \overline{\mathbb{R}^3} \rightarrow \mathbb{R}^{c_{out} \times c_{in}}$. $\overline{S^2}$ is the spherical coordinate, which can be visualized as the icosahedron vertices. $\overline{\mathbb{R}^3}$ is the spatial coordinate, which we design to be symmetric to \mathcal{I} . The kernel value is subject to constraint in (6), taking the same value anywhere on a circle around the z -axis.

4.3 Discretization of \mathbb{R}^3 in the convolution

As mentioned above, the domain of a kernel is $\overline{S^2} \times \overline{\mathbb{R}^3}$, where $\overline{\mathbb{R}^3}$ corresponds to the set of spatial coordinates of the kernel points. While the design choice of $\overline{\mathbb{R}^3}$ does not affect the equivariance property, it affects the querying position on the input feature map as shown in the last row of (5). By designing them properly, we can reduce computations in feature querying.

The idea is to design $\overline{\mathbb{R}^3}$ such that it is closed under actions of $\overline{\text{SO}(3)}$. In this way, we always have $R[i'_p]t[j'_q] = t[j''_q] \in \overline{\mathbb{R}^3}$ for some j''_q in (5). The features queried for a single $R[i'_p] \in \overline{S^2}$ can be reused for all $R[i] \in \overline{S^2}$ up to a permutation. Since the feature querying involves weighted sum over neighboring points which is pretty expensive, reducing the number of queries largely improves the efficiency.

In practice, we reuse the vertices of an icosahedron and the origin as the kernel points. We denote the set $\overline{S_0^2}$. This discretization also respects the equivariance constraint (6), since the 13 points lie on 5 circles centered around the z -axis. As a result, the discretized kernel $\kappa : \overline{S^2} \times \overline{S_0^2} \rightarrow \mathbb{R}^{c_{out} \times c_{in}}$ has $12 \times 5 = 60$ learnable $\mathbb{R}^{c_{out} \times c_{in}}$ weight matrices. The final convolution kernel is visualized in Fig. 2.

4.4 Nonlinear layer, pooling, and batch normalization

We use element-wise scalar nonlinearity (ReLU and leaky ReLU) in the network. The spatial pooling is by subsampling the input points and aggregating the features of neighboring input points to the subsampled points. Batch normalization is applied to normalize over the batch, $\overline{S^2}$, and \mathbb{R}^3 dimensions. All these choices follow the common practice of a conventional CNN (KPConv [20]) and G-CNN (EPN [12]). It maintains the equivariance because we use a trivial representation ρ of H . We also adopted the group attentive pooling in EPN to pool over the $\overline{S^2}$ dimension and generate $\overline{\text{SO}(3)}$ -invariant features.

4.5 Permutation layer for $\text{SO}(3)$ detection

Being able to decompose the group-invariant features and the group variations is the main advantage of group-equivariant learning. While we claimed $\text{SE}(3)$ recovery in Sec. 1, here we only discuss the detection in $\text{SO}(3)$ since the detection in \mathbb{R}^3 is already taken care of by conventional CNNs.

In a conventional CNN, one detects the location $x \in \mathbb{R}^n$ of an object by finding the location of the maximal response of a feature map defined on \mathbb{R}^n . Detecting the transformation $T \in G$ works in a similar way for a G-CNN by extending \mathbb{R}^n to G . However, it does not work for our network, because our feature map is defined on $\overline{S^2} = \overline{\text{SO}(3)}/\overline{\text{SO}(2)}$ which is a subspace of $\overline{\text{SO}(3)}$, and we adopted a trivial representation for $\text{SO}(2)$. It means that for the feature at a coordinate in $\overline{S^2}$, the information in $\text{SO}(2)$ is lost, and the feature is invariant to all planar rotations around a certain axis.

Nevertheless, we can recover the $\text{SO}(3)$ pose by viewing the feature map as a whole. Recall that $\overline{S^2}$ is a homogeneous space $\overline{\text{SO}(3)}$ and is closed under the actions of $\overline{\text{SO}(3)}$. Rewrite $\overline{S^2}$ as an ordered

Table 1: Efficiency comparison in terms of the GPU memory consumption and the running speed between EPN [12] and our method on three tasks. Two numbers are reported for *training/inference* respectively. \downarrow means lower is better. \uparrow means higher is better. The best is shown in bold font.

Tasks	ModelNet40 Pose		ModelNet40 Classification		3DMatch Keypoint Matching	
Methods	Memory (GB) \downarrow	Speed (fps) \uparrow	Memory (GB) \downarrow	Speed (fps) \uparrow	Memory (GB) \downarrow	Speed (fps) \uparrow
EPN [12]	22.2 / 16.9	1.1 / 1.6	24.9 / 12.7	1.2 / 0.9	37.4 / 8.5	0.6 / 3.1
<i>Ours</i>	4.3 / 2.8	6.7 / 11.1	10.5 / 7.4	4.3 / 5.1	6.2 / 2.4	3.7 / 23.6

set $\{R_{\mathbf{n}}[1], \dots, R_{\mathbf{n}}[12]\}$, the action of $R[i] \in \overline{\text{SO}(3)}$ follows:

$$R[i]\{R_{\mathbf{n}}[1], \dots, R_{\mathbf{n}}[12]\} = \{R_{\mathbf{n}}[m_i(1)], \dots, R_{\mathbf{n}}[m_i(12)]\} \quad (7)$$

is a permutation of the original ordered set where $R_{\mathbf{n}}[m_i(j)] = R[i]R_{\mathbf{n}}[j]$. We show in the appendix that there is an injection from $\overline{\text{SO}(3)}$ to the group of permutations of 12 elements, the symmetric group of degree 12, S_{12} . In other words, each element in $\overline{\text{SO}(3)}$ maps to a unique permutation of $\overline{S^2}$ as an ordered set.

We design a permutation layer to detect $\text{SO}(3)$ inspired from this observation. The permutations m_i for all $R[i] \in \overline{\text{SO}(3)}$ are precomputed, and applied on features of the 12 channels in the $\overline{S^2}$ dimension to generate 60 permutations of the feature map. An feature map of dimension $C \times |\overline{S^2}|$ is augmented to dimension $C \times |\overline{S^2}| \times |\overline{\text{SO}(3)}|$. Then we can detect the $\text{SO}(3)$ pose from the feature map across the $\overline{\text{SO}(3)}$ dimension. It also provides us another way to get $\text{SO}(3)$ -invariant features which is selecting the $C \times |\overline{S^2}|$ features corresponding to the correct pose. The selected feature is equivalent to the feature of the input point cloud under the canonical pose. While this operation increase the size of feature maps, it only needs to be applied once near the very end of the network and can be applied after global spatial-pooling. Therefore the computation overhead is limited.

4.6 Miscellaneous

Depending on the specific task, the prediction head has a slightly different design, which composes the last few layers of the network. The loss functions inherit from EPN [12], including cross-entropy loss for classifications, L2 loss for residual pose regression, and batch-hard triplet loss for keypoint matching. We refer to the appendix for more details about the prediction heads and the loss functions.

5 Experiments

The experiments follow those in a state-of-the-art $\text{SE}(3)$ -equivariant G-CNN, EPN [12], as our method and EPN are similar in several ways. They are both $\text{SE}(3)$ -equivariant point cloud networks with KPConv-style convolutions. They both use the icosahedral rotation group \mathcal{I} to discretize $\text{SO}(3)$. However, EPN is a G-CNN with features defined on $\mathcal{I} \times \mathbb{R}^3$, while our method works with features defined on the homogeneous space $\overline{S^2} \times \mathbb{R}^3$.

Two datasets, ModelNet40 [21] and 3DMatch [22], are used in the experiments. ModelNet40 is composed of 3D CAD models of 40 categories of objects. 3DMatch is a real-scan dataset of indoor scenes. For the ModelNet40 dataset, we conduct the pose estimation task and the classification and retrieval task. For the 3DMatch dataset, we conduct the keypoint matching task. We will briefly introduce the experiment setup below, and EPN [12] may be referred to for further details.

In Tab. 1, we list the GPU memory consumption and running speed of our method and EPN [12] in the three tasks. The comparisons are under the same input size, number of feature channels, and number of network layers. (The separable convolution of $\text{SO}(3)$ and \mathbb{R}^3 in EPN are together considered one layer.) The numbers are not comparable between training and inference because the batch size could be different (see the appendix). The specific configurations in each experiment are introduced later. All experiments are run on a single NVIDIA A40 GPU. We shall see that our network is much smaller and runs much faster in all three tasks, indicating the potential application value of our method. We boost the efficiency without sacrificing the performance, as is shown later.

Table 2: Experiment result on pose estimation on the ModelNet40 dataset. The mean, median, and max angular errors are shown for each method.

Methods	Mean ($^{\circ}$) \downarrow	Median ($^{\circ}$) \downarrow	Max ($^{\circ}$) \downarrow
KPCConv [20]	11.46	8.06	82.32
EPN [12]	1.25	1.11	6.63
Ours	1.17	1.08	5.90

Table 3: Experiment result on object classification and retrieval on the ModelNet40 dataset.

Methods	Acc (%) \uparrow	mAP (%) \uparrow
QENet [23]	74.4	-
PointNet [24]	83.6	-
PointNet++ [25]	85.0	70.3
DGCNN [26]	81.1	-
PointCNN [27]	84.5	-
KPCConv [20]	86.7	77.5
EPN [12]	88.3	79.7
<i>Ours</i> (with GA-pooling [12])	88.2	80.3
<i>Ours</i> (with permutation layer)	89.3	82.9

5.1 Pose Estimation on ModelNet40

In this experiment, the network takes a pair of point clouds of an object and predicts the relative rotation between them. The pair of point clouds are centered and different by an arbitrary rotation. To avoid the pose ambiguity of objects with rotational symmetric shapes, only the airplane category is used in this experiment, with 1,252 models in the training set and 101 models in the test set. A point cloud is generated by randomly subsampling 1,024 points on the object surface. The network is trained for 80k iterations with batch size 8.

The experiment result is shown in Tab. 2. We achieved better rotation estimation accuracy than EPN [12] overall. It shows that reducing the domain of feature maps does not compromise the capacity of the network to capture rotational variance. It also shows that we are able to detect the $SO(3)$ pose through the permutation layer. Besides, the equivariant networks perform better than a non-equivariant network KPCConv [20] by a large margin.

5.2 Classification and retrieval on ModelNet40

In this experiment, given a point cloud of an object, the network predicts its category. We also extract the features of objects, and retrieve the object that is the nearest neighbor in the feature space for each queried object. The goal is to retrieve an object of the same category. The evaluation metrics are the classification accuracy (Acc) and mean average precision (mAP) of retrieving an object of the correct category. This experiment is designed in ModelNet40 [21] and followed by EPN [12] and other existing work. Our network is trained with batch size 12 for 80k iterations.

The result is shown in Tab. 3. All results are trained and tested with rotational augmentation. The performance shows the ability of the networks to learn stable semantic features for each category of objects regardless of rotational variations. One may observe that non-equivariant neural networks also achieve decent performance with rotational augmentations in training. However, the equivariant networks EPN [12] and our method perform better, and ours performs the best in the list. It shows that our method is capable of learning $SE(3)$ -invariant and semantically-expressive features.

Ablation Since this task requires $SE(3)$ -invariant features, there are two options in our network: either using the group-attentive pooling introduced in EPN [12] to pool over the $\overline{S^2}$ dimensions or using the permutation layer to find the canonical permutation of $\overline{S^2}$ dimensions. Either way, the canonical pose of objects in ModelNet40 can be used to supervise the GA-pooling or the permutation. The result shows that the permutation layer yields better performance. The reason might be that the permutation layer stacks together features from $\overline{S^2}$ and preserves the most information.

Table 4: Experiment result of keypoint matching on the 3DMatch dataset. The numbers are the average recall (%), the higher the better. Notation * represents the result with given point normal information.

	SHOT[30]	3DM[22]	CGF[31]	PPFN[28]	PPFF[32]	3DSN[33]	Li[34]	Li[34]*	EPN[12]	<i>Ours</i>
Kitchen	74.3	58.3	60.3	89.7	78.7	97.5	92.1	99.4	99.0	99.4
Home 1	80.1	72.4	71.1	55.8	76.3	96.2	91.0	98.7	99.4	98.7
Home 2	70.7	61.5	56.7	59.1	61.5	93.2	85.6	94.7	96.2	96.6
Hotel 1	77.4	54.9	57.1	58.0	68.1	97.4	95.1	99.6	99.6	99.1
Hotel 2	72.1	48.1	53.8	57.7	71.2	92.8	91.3	100.0	97.1	98.1
Hotel 3	85.2	61.1	83.3	61.1	94.4	98.2	96.3	100.0	100.0	100.0
Study	64.0	51.7	37.7	53.4	62.0	95.0	91.8	95.5	96.2	95.2
MIT Lab	62.3	50.7	45.5	63.6	62.3	94.1	84.4	92.2	93.5	90.9
Average	73.3	57.3	58.2	62.3	71.8	95.6	91.0	97.5	97.6	97.3

5.3 Keypoint matching on 3DMatch

In this task, patches of point clouds extracted locally around keypoints in a large, dense scan are input to the network, and each mapped to a feature vector of 64-dim as the keypoint descriptor. Each patch has 1,024 points. Then we evaluate the average recall of keypoint correspondence across different scans through nearest neighbor search in the feature space, as proposed in PPFNet [28]. Our network is trained with 16 patches in a batch for 150k iterations, consistent with EPN [12].

This experiment’s performance in Tab. 4 indicates the capability of learning distinctive and rotation-invariant features for local patches of point clouds. Though not achieving the best in the list, our method delivers comparable performance to the top methods using only a fraction of computational resources as EPN [12]. We use the GA-pooling layer in this experiment because the permutation layer requires supervision on the pose, while a canonical pose is not defined for local patches of point clouds, and GA-pooling works with or without the pose supervision. However, the result shows that GA-pooling over the $|S^2|$ features also provides distinctive features for keypoint matching. This part may be further improved by taking the information of the global scan [28] or the matching scan [29] into consideration, in which case the permutation layer may get hints on the optimal permutation from the larger context. It goes beyond the focus of this paper and is left for future work.

6 Conclusion

This paper presents a new design of SE(3)-equivariant point cloud network. We develop a SE(3)-equivariant convolution that is efficient, simple, and expressive simultaneously by working with feature maps defined on the homogeneous space $S^2 \times \text{SO}(3)$ associated with the stabilizer SO(2) and using a trivial representation of SO(2). We further improve the efficiency of convolutions by designing the kernel points to be symmetric to the discretized rotation group $\overline{\text{SO}(3)}$. Moreover, we propose a permutation layer to recover $\overline{\text{SO}(3)}$ information from S^2 dimensions of features, so that the network is able to detect SO(3) rotations. Experiments show that our network delivers state-of-the-art performance in multiple tasks while consuming only a fraction of memory and computation resources as a G-CNN with similar performance. Our method can open exciting opportunities to introduce the SE(3)-equivariance property to mainstream point cloud networks for various tasks.

This work also has some limitations. We do not outperform EPN [12] in the keypoint matching task, implying that the network needs improvement when dealing with inputs without a clear pose definition. The requirement of pose supervision for the permutation layer could limit its application in certain tasks. While we made some design choices that turned out to work fine, whether or not they are optimal remains unknown. For example: Can we improve the design of the kernel points? What if we use a non-trivial representation of SO(2)? Are there other choices for the stabilizer? However, based on what we have done, we believe that the idea presented is meaningful and the benefit is substantial. Thus we leave these questions for future work. From a general perspective, our method starts by working on a new homogeneous space. It would be interesting to explore whether this strategy can be extended to other groups, which is also an attractive direction for future work.

References

- [1] T. S. Cohen, M. Geiger, J. Köhler, and M. Welling, “Spherical cnns,” *arXiv preprint arXiv:1801.10130*, 2018.
- [2] C. Esteves, C. Allen-Blanchette, A. Makadia, and K. Daniilidis, “Learning so (3) equivariant representations with spherical cnns,” in *Proceedings of the European Conference on Computer Vision (ECCV)*, 2018, pp. 52–68.
- [3] N. Thomas, T. Smidt, S. Kearnes, L. Yang, L. Li, K. Kohlhoff, and P. Riley, “Tensor field networks: Rotation-and translation-equivariant neural networks for 3d point clouds,” *arXiv preprint arXiv:1802.08219*, 2018.
- [4] T. Cohen and M. Welling, “Group equivariant convolutional networks,” in *International conference on machine learning*. PMLR, 2016, pp. 2990–2999.
- [5] E. Hoogeboom, J. W. Peters, T. S. Cohen, and M. Welling, “Hexaconv,” in *International Conference on Learning Representations*, 2018.
- [6] T. Ceccherini-Silberstein, A. Machì, F. Scarabotti, and F. Tolli, “Induced representations and Mackey theory,” *Journal of Mathematical Sciences*, vol. 156, no. 1, pp. 11–28, 2009.
- [7] T. S. Cohen and M. Welling, “Steerable cnns,” *arXiv preprint arXiv:1612.08498*, 2016.
- [8] T. S. Cohen, M. Geiger, and M. Weiler, “Intertwiners between induced representations (with applications to the theory of equivariant neural networks),” *arXiv preprint arXiv:1803.10743*, 2018.
- [9] M. J. Hutchinson, C. Le Lan, S. Zaidi, E. Dupont, Y. W. Teh, and H. Kim, “Lietransformer: Equivariant self-attention for lie groups,” in *International Conference on Machine Learning*. PMLR, 2021, pp. 4533–4543.
- [10] T. Cohen, M. Weiler, B. Kicanaoglu, and M. Welling, “Gauge equivariant convolutional networks and the icosahedral cnn,” in *International conference on Machine learning*. PMLR, 2019, pp. 1321–1330.
- [11] D. Worrall and G. Brostow, “Cubenet: Equivariance to 3d rotation and translation,” in *Proceedings of the European Conference on Computer Vision (ECCV)*, 2018, pp. 567–584.
- [12] H. Chen, S. Liu, W. Chen, H. Li, and R. Hill, “Equivariant point network for 3d point cloud analysis,” in *Proceedings of the IEEE/CVF Conference on Computer Vision and Pattern Recognition*, 2021, pp. 14 514–14 523.
- [13] M. Winkels and T. S. Cohen, “3d g-cnns for pulmonary nodule detection,” *arXiv preprint arXiv:1804.04656*, 2018.
- [14] E. J. Bekkers, “B-spline cnns on lie groups,” in *International Conference on Learning Representations*, 2019.
- [15] B. Hall, *Lie groups, Lie algebras, and representations: an elementary introduction*. Springer, 2015, vol. 222.
- [16] M. Weiler, M. Geiger, M. Welling, W. Boomsma, and T. S. Cohen, “3d steerable cnns: Learning rotationally equivariant features in volumetric data,” *Advances in Neural Information Processing Systems*, vol. 31, 2018.
- [17] F. Fuchs, D. Worrall, V. Fischer, and M. Welling, “Se (3)-transformers: 3d roto-translation equivariant attention networks,” *Advances in Neural Information Processing Systems*, vol. 33, pp. 1970–1981, 2020.
- [18] S. Batzner, A. Musaelian, L. Sun, M. Geiger, J. P. Mailoa, M. Kornbluth, N. Molinari, T. E. Smidt, and B. Kozinsky, “E (3)-equivariant graph neural networks for data-efficient and accurate interatomic potentials,” *Nature communications*, vol. 13, no. 1, pp. 1–11, 2022.
- [19] J. Brandstetter, R. Hesselink, E. van der Pol, E. Bekkers, and M. Welling, “Geometric and physical quantities improve e (3) equivariant message passing,” *arXiv preprint arXiv:2110.02905*, 2021.
- [20] H. Thomas, C. R. Qi, J.-E. Deschaud, B. Marcotegui, F. Goulette, and L. J. Guibas, “Kpconv: Flexible and deformable convolution for point clouds,” *Proceedings of the IEEE International Conference on Computer Vision*, 2019.

- [21] Z. Wu, S. Song, A. Khosla, F. Yu, L. Zhang, X. Tang, and J. Xiao, “3d shapenets: A deep representation for volumetric shapes,” in *Proceedings of the IEEE conference on computer vision and pattern recognition*, 2015, pp. 1912–1920.
- [22] A. Zeng, S. Song, M. Nießner, M. Fisher, J. Xiao, and T. Funkhouser. “3dmatch: Learning local geometric descriptors from rgb-d reconstructions,” in *Proceedings of the IEEE conference on computer vision and pattern recognition*, 2017, pp. 1802–1811.
- [23] Y. Zhao, T. Birdal, J. E. Lenssen, E. Menegatti, L. Guibas, and F. Tombari, “Quaternion equivariant capsule networks for 3d point clouds,” in *European Conference on Computer Vision*. Springer, 2020, pp. 1–19.
- [24] C. R. Qi, H. Su, K. Mo, and L. J. Guibas, “Pointnet: Deep learning on point sets for 3d classification and segmentation,” in *Proceedings of the IEEE conference on computer vision and pattern recognition*, 2017, pp. 652–660.
- [25] C. R. Qi, L. Yi, H. Su, and L. J. Guibas, “Pointnet++: Deep hierarchical feature learning on point sets in a metric space,” *Advances in neural information processing systems*, vol. 30, 2017.
- [26] Y. Wang, Y. Sun, Z. Liu, S. E. Sarma, M. M. Bronstein, and J. M. Solomon, “Dynamic graph cnn for learning on point clouds,” *Acm Transactions On Graphics (tog)*, vol. 38, no. 5, pp. 1–12, 2019.
- [27] Y. Li, R. Bu, M. Sun, W. Wu, X. Di, and B. Chen, “Pointcnn: Convolution on x-transformed points,” *Advances in neural information processing systems*, vol. 31, 2018.
- [28] H. Deng, T. Birdal, and S. Ilic, “Ppfnet: Global context aware local features for robust 3d point matching,” in *Proceedings of the IEEE conference on computer vision and pattern recognition*, 2018, pp. 195–205.
- [29] S. Huang, Z. Gojcic, M. Usvyatsov, A. Wieser, and K. Schindler, “Predator: Registration of 3d point clouds with low overlap,” in *Proceedings of the IEEE/CVF Conference on Computer Vision and Pattern Recognition*, 2021, pp. 4267–4276.
- [30] F. Tombari, S. Salti, and L. Di Stefano, “Unique shape context for 3d data description,” in *Proceedings of the ACM workshop on 3D object retrieval*, 2010, pp. 57–62.
- [31] M. Khoury, Q.-Y. Zhou, and V. Koltun, “Learning compact geometric features,” in *Proceedings of the IEEE international conference on computer vision*, 2017, pp. 153–161.
- [32] H. Deng, T. Birdal, and S. Ilic, “Ppf-foldnet: Unsupervised learning of rotation invariant 3d local descriptors,” in *Proceedings of the European Conference on Computer Vision (ECCV)*, 2018, pp. 602–618.
- [33] Z. Gojcic, C. Zhou, J. D. Wegner, and A. Wieser, “The perfect match: 3d point cloud matching with smoothed densities,” in *Proceedings of the IEEE/CVF Conference on Computer Vision and Pattern Recognition*, 2019, pp. 5545–5554.
- [34] L. Li, S. Zhu, H. Fu, P. Tan, and C.-L. Tai, “End-to-end learning local multi-view descriptors for 3d point clouds,” in *Proceedings of the IEEE/CVF Conference on Computer Vision and Pattern Recognition*, 2020, pp. 1919–1928.